Supplementary Material

Fits and simulations

To illustrate the main characteristics of NO autoxidation on the one hand and of NO escape from solution on the other we simulated the kinetics of formation and disappearance of DEA/NO, NO, and nitrite with the Tenua program (http://bililite.com/tenua). We also simulated how autoxidation-mediated and direct nitrosation by GSH affect those kinetics including the kinetics of GSNO formation. We used two models for the simulations, a simplified mechanism with only 6 steps, and a more complete mechanism consisting of 20 steps.

Mechanism 1

In the simplified mechanism we lumped groups of reactions that can be envisioned as rapid equilibria followed by slower steps together in single steps. The advantage of this approach is that it enables one to comprehend the dynamics of the system. The simplified model we used for the simulations is illustrated by Scheme S1.

Accordingly, we divided the autoxidation of NO in two reactions: slow oxidation leading from NO and O_2 to NO_2, and rapid hydrolysis leading from NO_2 to NO_2^- (yellow blocks in Scheme S1). The oxidation presents as a third-order reaction – second order in NO and first order in O_2; it is almost certainly not a true third order reaction, but rather of the rapid equilibrium type (A+B↔AB→P, with $k_d \gg k_p$ and [AB]<<[A],[B]). Irrespective of whether the initial complex is formed between two NO molecules or between NO and O_2, the kinetics are described by an apparent third-order rate constant of the type $k_{app}=K_a \cdot k_p$ with a value of $3.4 \cdot 10^6$ $M^{-2}s^{-1}$ at 37 °C [1].

The most important property of the hydrolysis is its rapidity in comparison to the

oxidation. Hence, it does not affect the overall kinetics other than by changing the stoichiometry of the reaction (from 2 NO/O_2 to 4 NO/O_2). Like the preceding oxidation, it is of the rapid-equilibrium type (at least in the absence of phosphate) with N_2O_3 formed from NO and NO_2 in rapid (but unfavorable) equilibrium and hydrolyzed in a slower step to H^+/NO_2^-. The rate constants for association, dissociation, and hydrolysis of N_2O_3 have been reported at 25°C [2]; from these an apparent rate constant for the overall reaction of $7 \cdot 10^6$ $M^{-1}s^{-1}$ can be derived.

In addition to autoxidation, and more important than that in the present study, NO disappears by escape from solution to the atmosphere. This is a simple first-order process, for which we applied a rate constant that yielded a best fit to the observed electrode decay kinetics.

In the presence of GSH, nitrosation is introduced into the scheme (pink blocks in Scheme S1). For autoxidation-mediated nitrosation, two competing mechanisms have been proposed. According to the older one, which still seems to be the mechanism favored by most researchers, N_2O_3 is the nitrosating species. According to the alternative view, advocated by us and several other groups, the more relevant mechanism starts by oxidation of GSH by NO_2, followed by rapid binding of NO to the $GS^{\bullet}$ radical. Although there are some mechanistic consequences tied in with the choice of mechanism (see below), it will not affect the interpretation of our results, because these processes all occur after the rate-limiting oxidative reaction and will therefore, if anything, only affect the stoichiometry of the reaction. Therefore, we treated autoxidation-mediated nitrosation in a simplified fashion. Since the rate with which the nitrosating species is produced is not affected by GSH, the crucial parameter in the process will be the ratio of the rate constants for hydrolysis and nitrosation, since that will determine the product distribution between nitrite and GSNO. Using this ratio, which has been determined previously [3] to be $4.15 \cdot 10^4$ M^{-1}, we calculated a value for the apparent
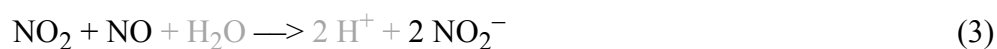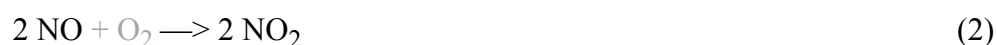
rate constant for nitrosation.

At this junction, we should point out that we are well aware that by cutting corners we introduced a couple of potential sources of error. Firstly, by calculating the apparent rate constant for nitrosation in this way, we tacitly assume that the reaction remains of the rapid equilibrium type. Strictly spoken, this is not true, as k_p may become of similar magnitude as k_d. Our simplification may therefore result in an overestimation of k_{app}, which will not increase linearly indefinitely, but will approach the limiting value k_p. However, this will not affect the overall autoxidation rate constant, which is determined completely by the preceding oxidation, and it will not affect product distribution between hydrolysis and nitrosation, which will still be determined by the ratio of the respective rate constants.

Secondly, although both mechanisms assume competition between hydrolytic and nitrosative pathways, they do so at different stages in the reaction: With N_2O_3 as nitrosating species, competition is between GSH and H_2O. Consequently, nitrosation will increase with the GSH concentration, but it will not be affected by the NO concentration. On the other hand, with NO_2/NO as the nitrosating species, competition is between GSH and NO: high concentrations of NO will divert NO_2 away from GSH oxidation towards N_2O_3 formation (which will inhibit NO_2/NO–mediated nitrosation, but will promote N_2O_3–mediated nitrosation); low concentrations of NO will result in GSH oxidation at the cost of GSNO formation. Again, these phenomena will not affect the overall rate of autoxidation+autoxidation-mediated nitrosation, but they may result in product distribution changing as a function of the NO concentration. However, with a ratio of rate constants of 41.5 we already assume that 97 % of NO autoxidation follows the nitrosative pathway. Consequently, any effect of [NO] could only make autoxidation-mediated nitrosation less efficient than we are assuming in our simulations; the same is true for any deviation of the actual rate constants under our experimental conditions from published values.

For 'direct' nitrosation, we assume a reaction between NO, O_2, and GSH. This reaction will present as a third-order reaction, first-order in each reactant, but is almost certainly of the rapid-equilibrium type. We can only speculate about the order in which the compounds react. Three initial complexes (between GSH and NO, between GSH and O_2, or between NO and O_2) are conceivable. The kinetics would be similar in each case. The rate constant for the reaction applied by us is derived from fits of the effect of GSH on the pre-Cu peak height and is therefore dependent on the value we estimated for the rate of NO escape from solution.

In summary, the complete model is described by the following equations (Tenua mechanism 1, see below):

$$DEA/NO \longrightarrow 1.5\ NO + DEA \tag{1}$$

$$2\ NO + O_2 \longrightarrow 2\ NO_2 \tag{2}$$

$$NO_2 + NO + H_2O \longrightarrow 2\ H^+ + 2\ NO_2^- \tag{3}$$

$$NO_2 + NO + GSH \longrightarrow GSNO + H^+ + NO_2^- \tag{4}$$

$$NO_{dissolved} \longrightarrow NO_{gaseous} \tag{5}$$

$$NO + O_2 + GSH \longrightarrow GSNO + H^+ + O_2^- \tag{6}$$

Products and reactants in grey were not specifically considered in the model; they were either ignored (DEA, H_2O, H^+, O_2^-), or incorporated in the (apparent) reaction rate constants (O_2 in k_2' and k_6', GSH in k_4' and k_6'). Please note that the presence of SOD in the experiments allows us to disregard O_2^- in the simulations. Incorporation of O_2 and GSH in the apparent rate constants presupposes that [NO]<<[O_2],[GSH]. Strictly speaking, this assumption is no longer valid at the highest [DEA/NO] concentrations in Figs. S2 and S3 (> 100 μM). However, to more clearly illustrate the different ways in which the alternative mechanisms (autoxidation vs. NO escape and autoxidation-mediated vs. direct nitrosation) are

affected by [DEA/NO], we chose not to take that into account. Please note that DEA/NO concentrations above 100 µM were not investigated in the present study. As a result of these simplifications, reactions 2, 3, and 4 are treated as second-order reactions, while reaction 6 is treated as a pseudo-first order reaction.

From the literature we adopted the following values for the rate constants:

$$k_1 = 5 \cdot 10^{-3} \text{ s}^{-1}$$

This is the value reported at 37 °C by Schmidt et al. [1].

$$k_2` = 750 \text{ M}^{-1}\text{s}^{-1}$$

This value was calculated from the rate constant of $13.6 \cdot 10^6 \text{ M}^{-2}\text{s}^{-1}$, published for NO autoxidation at 37 °C by Schmidt et al. [1], by multiplication with $[O_2] \sim 220$ µM and division by 4 to account for the NO/O_2 stoichiometry.

$$k_3 = 2 \cdot 10^7 \text{ M}^{-1}\text{s}^{-1}$$

Goldstein and Csapski reported values of $1.1 \cdot 10^9 \text{ M}^{-1}\text{s}^{-1}$, $8.1 \cdot 10^4 \text{ s}^{-1}$, and $5.3 \cdot 10^2 \text{ s}^{-1}$ for the rate of formation of N_2O_3 from NO_2 and NO, the rate of dissociation of N_2O_3 to NO_2 and NO, and the rate of hydrolysis of N_2O_3 to NO_2^-, respectively [2]. From these a value for the overall reaction of $k_3 = 7 \cdot 10^6 \text{ M}^{-1}\text{s}^{-1}$ at 25°C can be calculated. We assumed a ~3x higher value at 37°C; the actual value is not critical as long as $k_3 >> k_2`$.

$$k_4` = 8.3 \cdot 10^8 \text{ M}^{-1}\text{s}^{-1}$$

Keshive et al. reported a value for the ratio of the rate constants for nitrosation (k_4) and hydrolysis (k_3) of $4.15 \cdot 10^4 \text{ M}^{-1}$ [3]. The value of $k_4`$ is calculated by multiplication of this ratio with the value of k_3 and the concentration of GSH (1 mM).

As illustrated in Fig. S1, NO traces are not affected by autoxidation-mediated nitrosation (Fig. S1A), whereas direct nitrosation results in lower and earlier peaks (Fig. S1B).

Fig. S2 illustrates how the height of the NO peak increases linearly with the DEA/NO concentration if NO disappears by escape to the atmosphere, whereas this is not the case if NO disappears by autoxidation (Fig. S2C). This is because autoxidation, as a second order reaction, becomes more efficient at higher NO concentrations, and thus at higher DEA/NO concentrations, than the first-order formation of NO from DEA/NO. For NO escape this phenomenon does not occur, as NO diffusion and DEA/NO decomposition are both first order processes. Also, for NO autoxidation as the predominant reaction, the NO peak arrives earlier when the DEA/NO concentration is increased (Fig. S2B), whereas this does not occur in the case of NO escape (Fig. S2A).

Fig. S3 shows the effect of increasing the DEA/NO concentration on the GSNO yield after an incubation time of 12 min for autoxidation-mediated and direct nitrosation. In Panel A two extreme cases are simulated: in the one extreme autoxidation is neglected and all GSNO is formed by the direct reaction between NO and GSH, in the other NO escape from solution is neglected and all GSNO formation is autoxidation-mediated. In the case of a direct reaction, GSNO yields will increase linearly with the concentration of DEA/NO. This is because NO escape to solution and GSNO formation are both first-order reactions, so the DEA/NO concentration will not affect the relative GSNO yield. Since we are ignoring GSH oxidation in the simplified scheme, there are no competing reactions for autoxidation-mediated nitrosation in the absence of NO escape, so the final yield of GSNO should be the same in all cases (50% of NO formed, i.e. 75% of the initial DEA/NO concentration). Nevertheless, the simulation shows a strong downward deviation from linearity below 1 µM DEA/NO. The reason for this is that below 1 µM DEA/NO, with published values for the relevant rate constants, autoxidation becomes too slow to allow complete conversion of NO to GSNO, with an increasing fraction still present as NO after 12 minutes (see also Fig. S2A). When GSH oxidation is taken into account (Mechanism 2, see below), autoxidation-mediated

6

nitrosation becomes almost negligible at low NO concentrations, since distribution between nitrosation and oxidation is determined by competition between NO and GSH, respectively.

Panel B presents simulations for direct GSNO formation, autoxidation-mediated GSNO formation, and a combination of both processes, under conditions where NO disappears both by escape from solution and by autoxidation. This time the deviation from linearity for autoxidation-mediated nitrosation is even larger, because autoxidation has to compete with NO escape from solution, which diverts an ever larger fraction of NO away from autoxidation, and hence from GSNO formation, when the initial DEA/NO concentration decreases. The direct reaction still exhibits a linear dependence in the investigated concentration range, but becomes less efficient at higher concentrations, due to increased competition with autoxidation. The dependence remains linear over the whole concentration range if direct and autoxidation-mediated nitrosation are both taken into consideration.

Mechanism 2

We also performed simulations with an extended model without simplifications to account for additional reactions involving the glutathiyl radical that is formed in the NO_2/NO-mediated mechanism of nitrosation but is not explicitly present in the simplified mechanism (Fig. S4). Basically, this is the mechanism applied by Keszler et al. [4] with slight modifications (Tenua Mechanism 2, see below). As for Mechanism 1, GSH will lower the NO peak height and will be nitrosated efficiently in case of NO escape to the atmosphere and direct nitrosation (Fig. S4A). The more pronounced decrease of the NO peak height is due to the higher GSH concentration we applied in these simulations (2 instead of 1 mM).

Fig S4B shows simulations for strictly autoxidation-mediated processes. The most striking difference with the corresponding simulations with Mechanism 1 is the very low level of nitrosation (~20 nM) attained with Mechanism 2. This is due to competition between autoxidation-mediated nitrosation and the oxidative processes that result in GSSG formation.

7

This competition occurs at two branch points: first there is competition for NO_2 between NO (nitrosation/hydrolysis pathway, reaction E3 of Tenua Mechanism 2) and GSH (nitrosation/oxidation pathway, reaction E6), which will shift in favor of nitrosation/oxidation when the NO concentration decreases. At the second branch point there is again competition between NO (nitrosative pathway) and GSH (oxidative pathway), this time for the GS$^•$ radical (reactions E7 and E9, respectively). Consequently, for the low NO concentrations applied in the present study (≤ 1 μM) and with published rate constants for nitrosative and oxidative processes, autoxidation-mediated nitrosation is expected to be negligible. This phenomenon, combined with the observation of almost complete nitrosation in the present study, provides further strong support for direct nitrosation as the only relevant nitrosative mechanism at [NO] ≤ 1 μM. Fig. S4B also shows that GSH is actually expected to cause a slight increase of the NO peak height. This is explained by the scavenging of NO_2 by GSH at the first branch point, which will increase the lifetime of NO.

In the simulations shown in Figs. S4C and D we compare the effects of direct and autoxidation-mediated nitrosation, while allowing NO to disappear by both escape from solution and autoxidation. Comparison of Figs. S4A and S4C shows that the inclusion of autoxidation results in some nitrite formation at the expense of NO escape in the absence of GSH, whereas it hardly affects GSNO formation. Fig. S4D illustrates that autoxidation-mediated nitrosation remains negligible and GSH still causes a slight increase of the NO peak height when NO escape is included in the mechanism. When all reactions are included (Fig. S4E), the simulations are virtually identical to those in the absence of autoxidation-meditated nitrosation (Fig. S4C), indicating that although some autoxidation may occur in the absence of GSH, autoxidation-mediated reactions will not affect the efficiency of (direct) GSNO formation.

Fig. S5 illustrates the simulated effects of the DEA/NO concentration on NO peak height and position in the absence of GSH for Mechanism 2. It basically recapitulates the

results obtained with Mechanism 1, with a linear increase of the peak height and unaffected peak position for NO escape but not for NO autoxidation.

Fig. S6 shows the simulation with Mechanism 2 for the effect of the DEA/NO concentration on the NO peak height before and after $CuSO_4$ addition in the presence of GSH. Figs. S6A and B, which may be compared with Fig. S3 for Mechanism 1, confirm the linear increase of the GSNO yield with the DEA/NO concentrations for direct but not for autoxidation-mediated nitrosation. However, with Mechanism 2 the deviation from linearity for autoxidation-mediated nitrosation is much more pronounced. As discussed above (Fig. S4), this is explained by competition between GSH and NO for NO_2 and $GS^{\bullet}$, which will decrease the efficiency of nitrosation when the DEA/NO concentration is lowered. Fig. S6B also shows a strong deviation from linearity and even a decrease of the GSNO yield for direct nitrosation at DEA/NO concentrations of 100 µM and higher. The main cause of this phenomenon is that the oxygen concentration will become limiting when the initial DEA/NO concentration approaches the initial O_2 concentration. When this factor is eliminated by keeping $[O_2]$ constant, Mechanisms 1 and 2 yield very similar results for direct nitrosation (compare Figs. S6B and S3B). As with Mechanism 1, an approximately linear increase of the GSNO yield over the whole DEA/NO concentration range is expected when both direct and autoxidation-mediated nitrosation are taken into consideration.

Fig. S6C illustrates that the pre-Cu^{2+} peak in the presence of GSH is also expected to increase linearly with the DEA/NO concentration for direct nitrosation in the concentration range of interest ($\leq$ 1µM). The curve for autoxidation-mediated nitrosation below 1 µM essentially follows that in the absence of GSH, since GSH hardly affects the NO peak height under these conditions (see Fig. S4D).

Fig. S7 shows simulations in the presence and absence of SOD. For NO escape and direct nitrosation (Fig. S7A) omission of SOD causes a further decrease of the NO peak

height and a decrease by about 50 % of the GSNO yield. Concomitantly, GSSG, nitrite, and nitrate are formed in considerable amounts. These effects are caused by the reaction of O_2^-, formed in reaction E19, with a second molecule of NO (reaction E11), which reduces the GSNO-to-NO stoichiometry from 1 to 0.5 and gives rise to the formation of alternative products. For autoxidation-mediated processes, SOD omission also causes a decrease of the NO peak height, albeit to smaller extent; GSNO formation remains negligible. When all reactions are included, simulations are quite similar to those obtained with NO escape and direct nitrosation alone, illustrating once more the insignificance of autoxidation-mediated reactions in the presence of GSH under the present conditions (micromolar or less NO, millimolar GSH).

As shown in Fig. S8, the simulations with this model predict that, for autoxidation-mediated processes, even in the absence of SOD, GSH will hardly affect the NO peak, shifting it to a somewhat earlier time (from 316 to 293 s) and a slightly lower amplitude (from 0.921 to 0.872 μM, which constitutes a 5% decrease, Figs. S8A and B). In the presence of SOD (Fig. S8C), one actually observes an increase of the peak height and a shift toward a later time (1.017 μM at 364 s). This is explained by the fact that the slight decrease in Fig. S8B is completely due to reaction E11 between NO with O_2^- that is formed in reaction E10, and to consumption of NO by ${}^\bullet$OH and NO_2 (reactions E3 and E17), which are formed from homolysis of peroxynitrite (reaction E12). When O_2^- is scavenged by SOD (reaction E18), these NO consuming reactions are blocked and one is left with a shift from autoxidation, which consumes 4 NO/O_2, to GSH oxidation, which consumes only 2 NO/O_2. This is further illustrated by the simulation in Fig. S8D, where we blocked all reactions involving superoxide by setting the rate constant of peroxynitrite formation (reaction E11) to zero: this simulation yielded very similar results to that in Fig. S8C. The slightly higher NO peak (1.049 μM at 386

10

s) is explained by the fact that 10 µM SOD does not completely prevent peroxynitrite formation.

Fig. S9 shows best fits for the [NO] progress curves in the absence and presence of GSH. Observed progress curves in the absence of GSH showed a much faster disappearance of NO than expected on the basis of literature values for the rate constants of NO autoxidation (compare black and blue curves in Fig. S9A) and could not be fitted by variation of the rate constants for DEA/NO decay and NO autoxidation (reactions E1 and E2, red curve). By contrast, a good fit was obtained assuming that NO disappears by escape from solution (Fig. S9B), confirming that NO mainly disappears by diffusion. Similarly, when we tried to match the progress curves in the presence of GSH assuming autoxidation-mediated nitrosation, fits were poor and yielded unrealistic rate constants for NO autoxidation (Fig. S9C), whereas a good fit was obtained with direct nitrosation (Fig. S9D).

In summary, fits and simulations strongly support escape to solution as the main pathway of NO disappearance in the absence of GSH, and direct nitrosation as the exclusive pathway for GSNO formation under the conditions of the present study.

Fits to Fig. 8 of the main article

The dependence of the pre- and post-Cu^{2+} NO peaks on the concentration of GSH with DEA/NO (Fig. 8A of the main text) and PROLI/NO (Fig. 8B of the main text) were fitted to one or two hyperbolic functions, as appropriate. The line drawn through the GSNO-curve (post-Cu^{2+}) is a best fit to the function $[NO]_{peak} = \dfrac{b \bullet [GSH]}{a + [GSH]}$, in which **a** is the EC_{50} for GSH and **b** the maximal yield of GSNO. For the curve with DEA/NO in the presence of Mg^{2+}, two terms were required: $[NO]_{peak} = \dfrac{b_1 \bullet [GSH]}{a_1 + [GSH]} + \dfrac{b_2 \bullet [GSH]}{a_2 + [GSH]}$. The line drawn through the NO-

curve (pre-Cu^{2+}) is a best fit to the equation $[NO]_{peak} = c - \dfrac{b \cdot [GSH]}{a + [GSH]}$, in which **a** is the EC_{50}

for GSH, **b** is the decrease of the peak height at saturating [GSH], and **c** is the peak height in

the absence of GSH. For the curve of DEA/NO in the presence of Mg^{2+}, two terms were

required: $[NO]_{peak} = c - \dfrac{b_1 \cdot [GSH]}{a_1 + [GSH]} - \dfrac{(c - b_1) \cdot [GSH]}{a_2 + [GSH]}$. Fitting parameters: DEA/NO, +Mg^{2+},

pre-Cu^{2+}: a_1=0.028±0.033 mM, a_2=4.0±2.1 mM, b_1=0.19±0.07 µM, and **c**=0.75±0.03 µM;

DEA/NO, +Mg^{2+}, post-Cu^{2+}: a_1=0.0082±0.0039 mM, a_2=1.35±0.85 mM, b_1=0.14±0.03 µM,

and b_2=1.22±0.38 µM; DEA/NO, –Mg^{2+}, pre-Cu^{2+}: **a**=0.041±0.038 mM, **b**=0.122±0.028 µM,

and **c**=0.71±0.02 µM; DEA/NO, –Mg^{2+}, post-Cu^{2+}: **a**=0.035±0.011 mM, and **b**=0.200±0.017

µM; PROLI/NO, +Mg^{2+}, pre-Cu^{2+}: **a**=2.14±1.77 mM, **b**=1.24±0.56 µM, and **c**=1.26±0.05

µM; PROLI/NO, +Mg^{2+}, post-Cu^{2+}: **a**=2.34±1.43 mM and **b**=1.28±0.65 µM.

Additional experiments

Fig. S10 shows the influence of NAD^+ and NADH on the NO progress curves

originating from 1 µM DEA/NO. In the absence of GSH, we observed slightly lower pre-Cu^{2+}

peak heights after omission of NAD^+ or substitution by NADH (results with 1 mM NAD^+, 1

mM NADH, and without NAD(H), respectively: 0.900±0.003, 0.798±0.019, and

0.840±0.014). In the presence of GSH, the pre-Cu^{2+} peak seemed to increase slightly when

NAD^+ was omitted or replaced with NADH (results with 1 mM NAD^+, 1 mM NADH, and

without NAD(H), respectively: 0.259±0.018, 0.317±0.020, and 0.293±0.029), whereas the

post-Cu^{2+} peak slightly decreased (results with 1 mM NAD^+, 1 mM NADH, and without

NAD(H), respectively: 0.873±0.018, 0.720±0.012, and 0.847±0.024).

Since we started these studies with a system containing NAD^+, many of the experiments that are presented in the main text in the absence of NAD^+, were originally performed in its presence. Fig. S11 summarizes these early results, which basically constitute a complete data set duplicating the results of the main paper. GSH caused a pronounced decrease of the NO peak height accompanied by formation of GSNO (Figs. S11A & B). The pre-Cu^{2+} peak height increased linearly with the DEA/NO concentration, while the peak position remained constant (Figs. 11C, D, & E). The post-Cu^{2+} peak also increased linearly with the DEA/NO concentration (Figs. S11F & G). The NO peak in the absence of GSH was not affected by Mg^{2+} or Ca^{2+}, whereas in the presence of GSH both divalent cations amplified the decrease of the pre-Cu^{2+} peak and the increase of the post-Cu^{2+} peak.

Fig. S12 shows the effects of Mg^{2+} on pre- and post-Cu^{2+} peak heights in the presence of NAC or β-ME. It demonstrates that Mg^{2+} lowers the NO peak height, while increasing the GSNO yield for both thiols, though perhaps not to quite the same extent as with GSH.

References

 [1] Schmidt, K.; Desch, W.; Klatt, P.; Kukovetz, W. R.; Mayer, B. *Naunyn-Schmiedeberg's Arch. Pharmacol.* **355**: 457-462; 1997.

[2] Goldstein, S.; Czapski, G. *J. Am. Chem. Soc.* **118**: 3419-3425; 1996.

[3] Keshive, M.; Singh, S.; Wishnok, J. S.; Tannenbaum, S. R.; Deen, W. M. *Chem. Res. Toxicol.* **9**: 988-993; 1996.

[4] Keszler, A.; Zhang, Y.; Hogg, N. *Free Radic. Biol. Med.* **48**: 55-64; 2010.

Simulation and fitting programs:

Tenua Mechanism 1:	**Reaction:**
DEANO <-> NO;	1
NO + NO <-> NO2 + NO2;	2
NO2 + NO <-> Nitrite + Nitrite;	3
NO2 + NO <-> GSNO + Nitrite;	4
NO <-> gas;	5
NO <-> GSNO;	6
rate(DEANO) = -0.67*k(+1)*DEANO;	#

*script

mechanism.solver = "stiff";

go;

(*timeStep 1.0; epsilon 0.01*)

 # This command is necessary to allow a 3/2 NO:DEA/NO stoichiometry. Consequently, we applied a rate constant in the simulations of 0.078 s^{-1}, corresponding to 1.5x the rate constant for DEA/NO decay that is reported in the literature and indicated in the Figure Legends (0.052 s^{-1}).

Tenua Mechanism 2:	Reaction:
DEANO <-> NO;	E1
2NO + O2 <-> 2 NO2;	E2
NO + NO2 <-> N2O3;	E3
N2O3 <-> 2 HNO2;	E4
N2O3 + GSH <-> GSNO + HNO2;	E5
NO2 + GSH <-> GS + HNO2;	E6
GS + NO <-> GSNO;	E7
GS + GS <-> GSSG;	E8
GS + GSH <-> GSSGH;	E9
GSSGH + O2 <-> GSSG + HO2;	E10
NO + HO2 <-> HONO2;	E11
HONO2 <-> HNO3;	E12
HONO2 <-> OH + NO2;	E13
HONO2 + GSH <-> GSOH + HNO2;	E14
GSOH + GSH <-> GSSG;	E15
OH + GSH <-> GS;	E16
OH + NO <-> HNO2;	E17
HO2 + SOD <-> H2O2 + SOD;	E18
NO + O2 + GSH <-> GSNO + HO2;	E19
NO <-> gas;	E20
rate(DEANO) = -0.67*k(+1)*DEANO;	#

*script

mechanism.solver = "stiff";

go;

Supplementary figure legends

Figure S1. Simulation with Mechanism 1 of the effect of GSH on the concentrations of DEA/NO and its metabolites in the case of (A) NO autoxidation and (B) NO escape from solution.

Shown are the simulated concentrations of DEA/NO (black), NO (red), NO_2^- (blue), and GSNO (green), with (dotted) and without (continuous) GSH. The curves with and without GSH for DEA/NO are superimposed, as are the curves for NO in Panel A. Simulation parameters (A): $k_1 = 5 \cdot 10^{-3}$ s^{-1}; $k_2{}' = 750$ $M^{-1}s^{-1}$; $k_3 = 2 \cdot 10^7$ $M^{-1}s^{-1}$; $k_4{}' = 0$ or $8.3 \cdot 10^8$ $M^{-1}s^{-1}$; (B): $k_1 = 5 \cdot 10^{-3}$ s^{-1}; $k_5 = 2 \cdot 10^{-3}$ s^{-1}; $k_6{}' = 0$ or $5 \cdot 10^{-3}$ s^{-1}; both: $[DEA/NO]_0 = 1$ µM. Simulations and fits in these and the following figures were performed with the Tenua program (http://bililite.com/tenua) according to Mechanism 1.

Figure S2. Simulation with Mechanism 1 of the effect of the concentrations of DEA/NO on the height and position of the NO peak.

Panels A and B show the simulated concentrations of DEA/NO (black) and NO (red) for initial concentrations of 0.67 (continuous) and 6.7 (dotted) µM DEA/NO, assuming that NO disappears by escape from solution or by autoxidation, respectively. Note the shift in peak position in case of NO autoxidation (panel B). Panel C shows the dependence of peak height on the DEA/NO concentration for NO autoxidation (red) and NO escape (blue). Best fits of the simulated peak heights in the concentration range investigated in the present study ($\leq$ 1µM) to the power function $y = b \cdot x^a$ are included as black dotted lines. For NO escape this line is superimposed on the simulated curve. Fitting parameters for a were 0.823±0.011 for autoxidation-mediated NO disappearance (0.599±0.009 if the complete curve was taken into account) and 0.984±0.008 for diffusion-mediated NO disappearance (0.99982±0.00005 for the whole curve). Simulation parameters (A): $k_1 = 5 \cdot 10^{-3}$ s^{-1}; $k_5 = 5 \cdot 10^{-3}$ s^{-1}; (B): $k_1 = 5 \cdot 10^{-3}$ s^{-1}; $k_2{}' = 750$ $M^{-1}s^{-1}$; $k_3 = 2 \cdot 10^7$ $M^{-1}s^{-1}$; both: $[DEA/NO]_0 = 0.67$ or 6.7 µM.

Figure S3. Simulation with Mechanism 1 of the effect of the concentrations of DEA/NO on the GSNO yield after 12 minutes.

Panel A shows the simulated dependence on the DEA/NO concentration of Cu^{2+}-mediated NO release after 12 minutes of incubation if (i) all GSNO is formed by autoxidation and NO escape from solution is negligible (red) or (ii) all GSNO is formed by a direct reaction between NO and GSH and NO autoxidation is negligible (blue). Data in the concentration range investigated in the present paper ($\leq 1\mu M$) were fitted to the power function $y = b \cdot x^a$ (black dotted lines, for direct nitrosation superimposed on the simulated curve). Fitting parameters for a were 1.53±0.04 for autoxidation-mediated NO disappearance (1.029±0.005 if the complete curve was taken into account) and 1 for diffusion-mediated NO disappearance. Panel B shows the simulated dependence on the DEA/NO concentration of Cu^{2+}-mediated NO release after 12 minutes of incubation if (i) GSNO is only formed by autoxidation (red) or (ii) by a direct reaction between NO and GSH (blue), and NO disappearing by both autoxidation and escape to solution. Also shown is the dependence when GSNO is formed both directly and by autoxidation (green dashes). Data in the concentration range investigated in the present paper ($\leq 1\mu M$) were fitted to the power function (black dotted lines, for direct nitrosation and the combination superimposed on the simulated curve). Fitting parameters for a were 1.77±0.03 for autoxidation-mediated NO disappearance (1.059±0.005 if the complete curve was taken into account), 0.994±0.003 for direct nitrosation (0.645±0.013 if the complete curve was taken into account), and 1.002±0.005 for a combination of direct and autoxidation-mediated GSNO formation (0.9426±0.0012 for the complete curve). (A): $k_1 = 5 \cdot 10^{-3}$ s^{-1}; $k_2' = 750$ M^{-1}s^{-1} <u>or</u> $k_5 = 5 \cdot 10^{-3}$ s^{-1}; $k_3 = 2 \cdot 10^7$ M^{-1}s^{-1}; $k_4' = 8.3 \cdot 10^8$ M^{-1}s^{-1}; $k_6' = 5 \cdot 10^{-3}$ s^{-1}; (B): $k_1 = 5 \cdot 10^{-3}$ s^{-1}; $k_2' = 750$ M^{-1}s^{-1} <u>and</u> $k_5 = 5 \cdot 10^{-3}$ s^{-1}; $k_3 = 2 \cdot 10^7$ M^{-1}s^{-1}; $k_4' = 8.3 \cdot 10^8$ M^{-1}s^{-1}; $k_6' = 5 \cdot 10^{-3}$ s^{-1}. We also simulated the autoxidation-mediated reaction to the more detailed Mechanism 2, which allows for GSH oxidation to GSSG (Panel A, crosses and dashed line see also Fig. S6). This simulation gave very low GSNO yields. Fitting parameter a was 2.34±0.05 for DEA/NO concentrations up to 1 μM, and 1.206±0.008 for the complete curve. See the legends to Fig. S6 for the applied rate constants.

Figure S4. Simulation with Mechanism 2 of the effect of GSH on the concentrations of DEA/NO and its metabolites.

Panel A: no autoxidation or autoxidation-mediated nitrosation; Panel B: no NO escape from solution or direct nitrosation; Panel C: no autoxidation-mediated nitrosation; Panel D: no direct nitrosation; Panel E: all reactions included. Continuous and dotted traces are in the absence and presence of 2 mM GSH, respectively. The following colors were used: black, DEA/NO; red, NO; yellow: NO escape from solution; blue: nitrite; green: GSNO; purple: GSSG; orange: nitrate. See text for details. Simulation parameters: $k_1 = 5.2 \cdot 10^{-3}$ s^{-1}; $k_2 = 3.2 \cdot 10^6$ M^{-2}s^{-1} or 0 (Panel A); $k_3 = 1.1 \cdot 10^9$ M^{-1}s^{-1}; $k_{-3} = 8.1 \cdot 10^4$ s^{-1}; $k_4 = 5.3 \cdot 10^2$ s^{-1}; $k_5 = 6.6 \cdot 10^7$ M^{-1}s^{-1} or 0 (Panels A and C); $k_6 = 2.2 \cdot 10^7$ M^{-1}s^{-1}; $k_7 = 3 \cdot 10^9$ M^{-1}s^{-1} or 0 (Panels A and C); $k_8 = 1 \cdot 10^9$ M^{-1}s^{-1}; $k_9 = 7 \cdot 10^7$ M^{-1}s^{-1}; $k_{-9} = 2.3 \cdot 10^5$ s^{-1}; $k_{10} = 5 \cdot 10^9$ M^{-1}s^{-1}; $k_{11} = 5 \cdot 10^9$ M^{-1}s^{-1}; $k_{12} = 0.9$ s^{-1}; $k_{13} = 0.35$ s^{-1}; $k_{14} = 6.6 \cdot 10^2$ M^{-1}s^{-1}; $k_{15} = 1 \cdot 10^5$ M^{-1}s^{-1}; $k_{16} = 1 \cdot 10^9$ M^{-1}s^{-1}; $k_{17} = 1 \cdot 10^9$ M^{-1}s^{-1}; $k_{18} = 2 \cdot 10^9$ M^{-1}s^{-1}; $k_{19} = 5 \cdot 10^4$ M^{-2}s^{-1} or 0 (Panels B and D); $k_{20} = 5 \cdot 10^{-3}$ s^{-1} or 0 (Panel B); [DEA/NO]$_0$ = 1 μM; [O$_2$]$_0$ = 0.22 mM; [GSH]$_0$ = 0 or 2 mM; [SOD]$_0$ = 10 μM.

Figure S5. Simulation with Mechanism 2 of the effect of the concentrations of DEA/NO on the height and position of the NO peak.

Panels A and B show the simulated concentrations of DEA/NO (black) and NO (red) for initial concentrations of 1 (continuous) and 10 (dotted) μM DEA/NO, assuming that NO disappears by escape from solution or by autoxidation, respectively. Note the shift in peak position in case of NO autoxidation (panel B). Panel C shows the dependence of peak height on the DEA/NO concentration for NO autoxidation (red) and NO escape (blue). Best fits of the simulated peak heights in the concentration range investigated in the present study ($\leq$ 1μM) to the power function $y = b \cdot x^a$ are included as black dotted lines. For NO escape this line is superimposed on the simulated curve. Fitting parameters for a were 0.834±0.012 for autoxidation-mediated NO disappearance and 0.99982±0.00008 for diffusion-mediated NO disappearance. Panel C shows the dependence of the time when [NO] reaches its maximum on the DEA/NO concentration. Simulation parameters as in Fig. S5.

Figure S6. Simulation with Mechanism 2 of the effect of the concentrations of DEA/NO on the GSNO yield after 12 minutes.

Panel A shows the simulated dependence on the DEA/NO concentration of Cu^{2+}-mediated NO release in the presence of 2 mM GSH after 12 minutes of incubation if (i) all GSNO is formed by autoxidation and NO escape from solution is negligible (red) or (ii) all GSNO is formed by a direct reaction between NO and GSH and NO autoxidation is negligible (blue). Data in the concentration range investigated in the present paper ($\leq 1\mu M$) were fitted to the power function $y = b \cdot x^{a}$ (black dotted lines, for direct nitrosation superimposed on the simulated curve). Fitting parameters for a were 2.34±0.03 for autoxidation-mediated NO and 0.996±0.006 for diffusion-mediated NO disappearance. Panel B shows the simulated dependence on the DEA/NO concentration of Cu^{2+}-mediated NO release after 12 minutes of incubation if NO disappears by both autoxidation and escape to solution and GSNO is only formed by (i) autoxidation (red), (ii) by a direct reaction between NO and GSH (blue), or (iii) by both (green). Data in the concentration range investigated in the present paper ($\leq 1\mu M$) were fitted to the power function (black dotted lines, for direct nitrosation and the combination superimposed on the simulated curve). Simulations with dashed lines (only visible in case of direct nitrosation) and open symbols were obtained with the unmodified Mechanism 2. In the simulations with continuous lines and closed symbols $[O_2]$ and [GSH] were kept constant (by inclusion of O_2 as a product in Reactions E2, E10, and E19, and by inclusion of GSH as a product in Reactions E5, E6, E9, E14, E15, E16, and E19). by including these reactants as a product in   Fitting parameters for a were 2.77±0.05 for autoxidation-mediated NO disappearance, 0.989±0.006 for direct nitrosation, and 0.994±0.010 for a combination of direct and autoxidation-mediated GSNO formation. Panel C shows the DEA/NO dependence of the pre-Cu NO peak heights in case of direct nitrosation (blue, with k_5, k_7=0) and autoxidation-mediated nitrosation (red, with k_{19}=0). Fitting parameters for b were 0.991±0.009 for autoxidation-mediated nitrosation and 0.981±0.002 for direct nitrosation. Fitting parameters as in Fig. S5.

Figure S7. Simulation with Mechanism 2 of the effect of omission of SOD on the concentrations of DEA/NO and its metabolites in the presence of GSH.

Panel A: no autoxidation or autoxidation-mediated nitrosation; Panel B: no NO escape from solution or direct nitrosation; Panel C: all reactions included. Continuous and dotted traces are

in the presence and absence of 10 μM SOD, respectively. Colour code and simulatrion pareameters as in Fig. S5. See text for details.

Figure S8. Simulation with Mechanism 2: SOD minimally affects autoxidation-mediated NO peak-heights.

Panels A and B show the simulated concentrations of DEA/NO, NO, nitrite, nitrate, GSNO, and GSSG in the absence (panel A) and presence (panel B) of GSH but in the absence of SOD for the extended mechanism 2 (see above). Panel C shows a simulation for the same mechanism in the presence of GSH and SOD. Panel D shows a simulation for the same mechanism as in Panel B, except that the rate of peroxynitrite formation was set to zero, precluding NO consumption by superoxide and metabolites of peroxynitrite. See text for details. Simulation parameters: $k_1 = 5.2 \cdot 10^{-3}$ s^{-1}; $k_2 = 2 \cdot 10^6$ M^{-2}s^{-1}; $k_3 = 1.1 \cdot 10^9$ M^{-1}s^{-1}; $k_{-3} = 8.1 \cdot 10^4$ s^{-1}; $k_4 = 5.3 \cdot 10^2$ s^{-1}; $k_5 = 6.6 \cdot 10^7$ M^{-1}s^{-1}; $k_6 = 2.2 \cdot 10^7$ M^{-1}s^{-1}; $k_7 = 3 \cdot 10^9$ M^{-1}s^{-1}; $k_8 = 1 \cdot 10^9$ M^{-1}s^{-1}; $k_9 = 7 \cdot 10^7$ M^{-1}s^{-1}; $k_{-9} = 2.3 \cdot 10^5$ s^{-1}; $k_{10} = 5 \cdot 10^9$ M^{-1}s^{-1}; $k_{11} = 5 \cdot 10^9$ M^{-1}s^{-1}; $k_{12} = 0.9$ s^{-1}; $k_{13} = 0.35$ s^{-1}; $k_{14} = 6.6 \cdot 10^2$ M^{-1}s^{-1}; $k_{15} = 1 \cdot 10^5$ M^{-1}s^{-1}; $k_{16} = 1 \cdot 10^9$ M^{-1}s^{-1}; $k_{17} = 1 \cdot 10^9$ M^{-1}s^{-1}; $k_{18} = 2 \cdot 10^9$ M^{-1}s^{-1}; [DEA/NO]$_0 = 1$ μM; [O$_2$]$_0 = 0.22$ mM; [GSH]$_0 = 1$ mM (Panels B, C, and D) or 0 mM (Panel A); [SOD]$_0 = 10$ μM (Panel C) or 0 μM (Panels A, B, and D).

Figure S9. Fits of the observed NO time curves in the absence and presence of GSH.

Panels A and B show experimental NO time curves (black) observed with 1 μM DEA/NO, together with best fits (red) for disappearance of NO by autoxidation (panel A) and escape from solution (panel B) in the absence of GSH. Panel A also shows a simulated curve (blue) obtained with literature values. Fitting parameters (A): $k_1 = 8.7 \cdot 10^{-3}$ s^{-1}; $k_2 = 6.8 \cdot 10^6$ M^{-2}s^{-1}; the blue curve was simulated with $k_1 = 5.2 \cdot 10^{-3}$ s^{-1} and $k_2 = 2.8 \cdot 10^6$ M^{-2}s^{-1}; (B): $k_1 = 1.0 \cdot 10^{-2}$ s^{-1}; $k_{20} = 4.9 \cdot 10^{-3}$ s^{-1}; all other parameters as in Fig. S5. Panels C and D show the corresponding curves and fits in the presence of 2 mM GSH for autoxidation-mediated NO consumption and nitrosation (panel C) and NO escape with direct nitrosation ((panel D). Fitting parameters: (C): $k_1 = 8.7 \cdot 10^{-3}$ s^{-1}; $k_2 = 3.6 \cdot 10^8$ M^{-2}s^{-1} (!); (D): $k_1 = 1.0 \cdot 10^{-2}$ s^{-1}; $k_{20} = 4.9 \cdot 10^{-3}$ s^{-1}; $k_{19} = 6.2 \cdot 10^4$ M^{-2}s^{-1}; all other parameters as in Fig. S5.

Figure S10. Effect of NAD$^+$ and NADH on pre- and post-Cu^{2+} DEA/NO-derived NO peaks in the absence and presence of GSH.

NO peak heights were determined from traces as in Fig. 1. Experimental conditions: 1 μM DEA/NO, 2 mM GSH as indicated, 4 mM CuSO$_4$, 1000 U/mL SOD, 0.1 mM DTPA, 5 mM MgCl$_2$, and 1 mM NAD$^+$ or NADH as indicated in 50 mM triethanolamine•HCl buffer (pH 7.4) in 0.5 mL at 37 °C; $n \geq 3$.

Figure S11. Nitrosation of GSH by glutathione in the presence of NAD$^+$.

Panel A: NO release curves from DEA/NO, added at $t = 0$, in the absence and presence of GSH, and the effect of CuSO$_4$ added after 12 minutes (indicated by the arrow). Panel B: Comparison of pre and post-Cu^{2+} peak heights in the absence and presence of GSH. Panel C-E: Correlation between NO peak heights and DEA/NO concentrations in the absence of GSH. Panel C shows NO time traces observed with 30, 200, 400, and 1000 nM DEA/NO. Panel D shows peak heights observed with a range of DEA/NO concentrations between 10 nM and 1 μM ($n = 3$). Data were fitted (dashed lines) to the equation $y = b \cdot x^a$. The observed value for a is very close to 1 (0.971±0.008), indicating a linear relationship between peak height and DEA/NO concentration. Panel E: Time at which the NO concentration is maximal for different DEA/NO concentrations. Panels F&G: Correlation between post Cu^{2+}-peak heights and DEA/NO concentrations in the presence of GSH. Panel F: NO time traces observed with 50, 200, 400, and 1000 nM DEA/NO. Panel G: Peak heights observed for DEA/NO concentrations between 20 nM and 1 μM ($n = 3$). Data were fitted (dashed lines) to the equation $b \cdot x^a$. The fit is linear with a very close to 1 (0.949±0.007), indicating a linear relationship between peak height and DEA/NO concentration. Panel H: Effect of Mg^{2+} and Ca^{2+} on DEA/NO decomposition and GSNO formation. Peak heights ($n = 5$) in the presence and absence of 5 mM MgCl$_2$ or CaCl$_2$: black columns, pre-Cu^{2+} without GSH; white columns, pre-Cu^{2+} with GSH; post-Cu^{2+} with GSH. Experimental conditions for all panels: 1

μM DEA/NO or as indicated, 2 mM GSH or as indicated, 4 mM $CuSO_4$ as indicated, 1000

U/mL SOD, 0.1 mM DTPA, 1 mM NAD^+, and 50 mM TEA (pH 7.4) in 0.5 mL at 37 °C.

Figure S12. Effect of Mg^{2+} on pre- and post-Cu^{2+} DEA/NO-derived NO peaks in the presence of NAC or β-ME.

NO peak heights were determined from traces as in Fig. 1. Experimental conditions: 1 μM DEA/NO, 1 mM NAC or β-ME as indicated, 4 mM $CuSO_4$, 1000 U/mL SOD, 0.1 mM DTPA, and 5 mM $MgCl_2$ as indicated in 50 mM triethanolamine•HCl buffer (pH 7.4) in 0.5 mL at 37 °C; $n≥3$.

Scheme S1. Schematic summary of the reactions considered in the comparison of direct and autoxidation-mediated nitrosation.

Autoxidation (yellow boxes) is treated as consisting of two modules (oxidation and hydrolysis). Nitrosation (pink boxes) is either direct, in which case it competes with autoxidation and escape to the atmosphere, or autoxidation-mediated, in which case it competes with hydrolysis. Apparent rate constants are indicated in red.

Figure S1. Simulation with Mechanism 1 of the effect of GSH on the concentrations of DEA/NO and its metabolites.
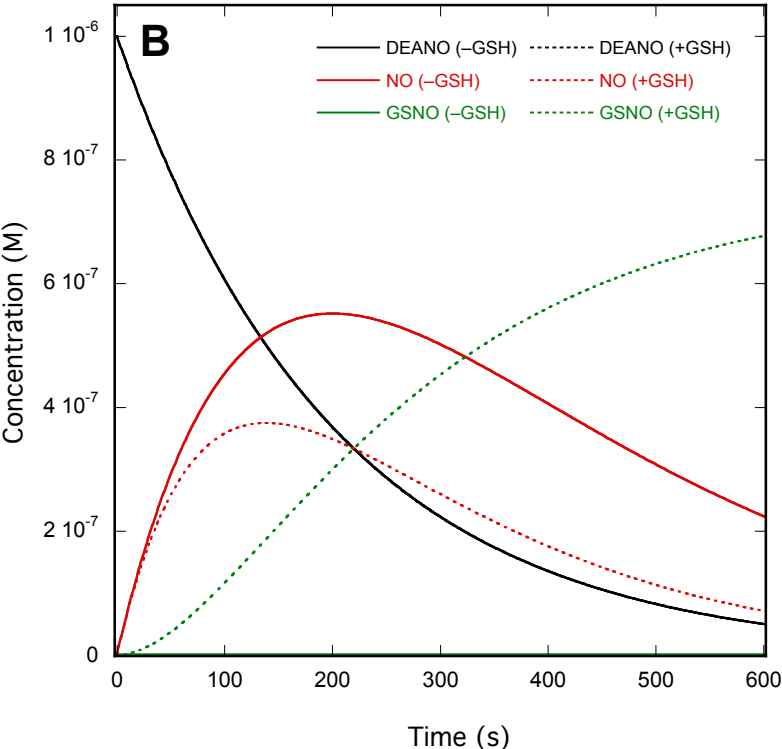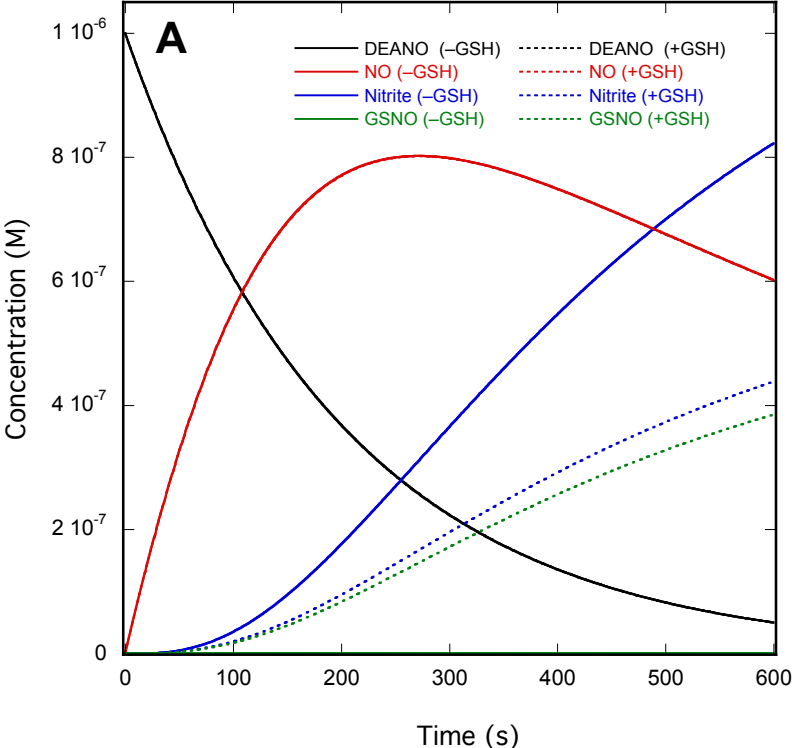
Figure S2. Simulation with Mechanism 1 of the effect of the concentrations of DEA/NO on the height and position of the NO peak.
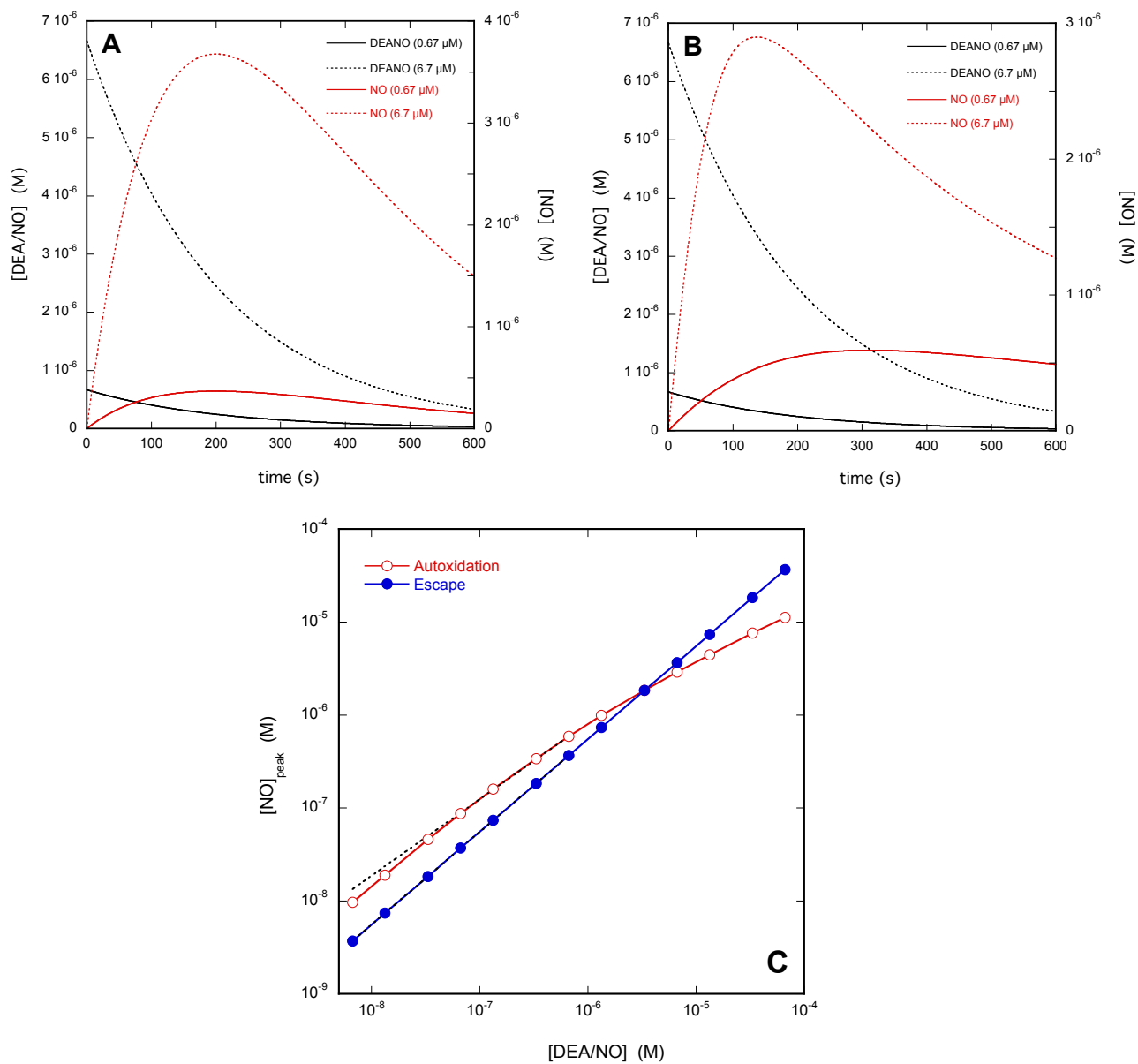
Figure S3. Simulation with Mechanism 1 of the effect of the concentrations of DEA/NO on the GSNO yield after 12 minutes.
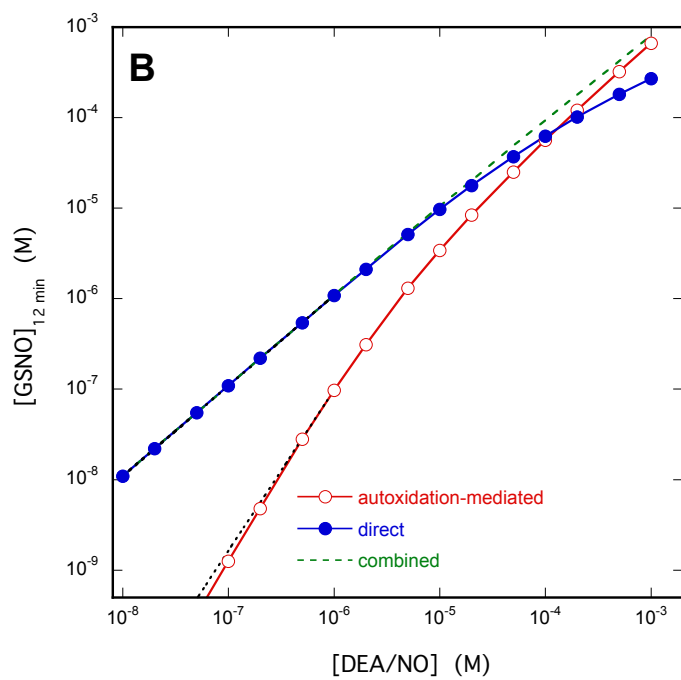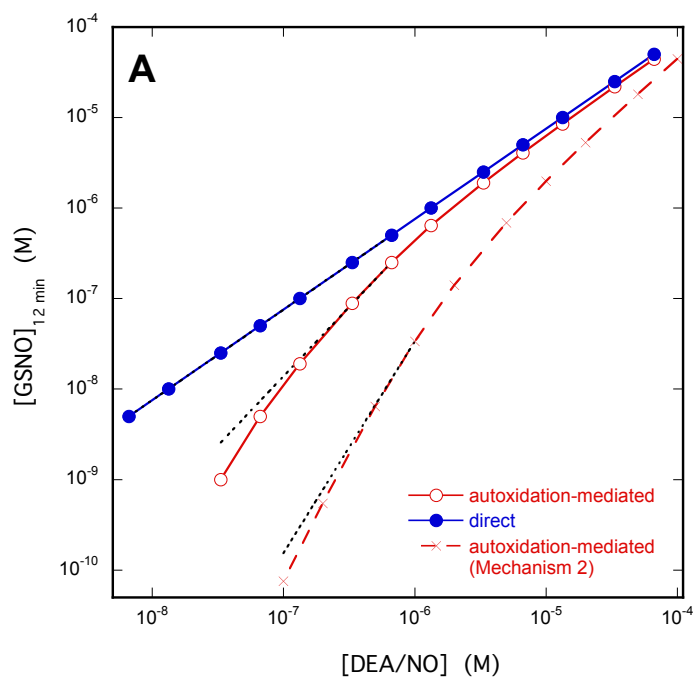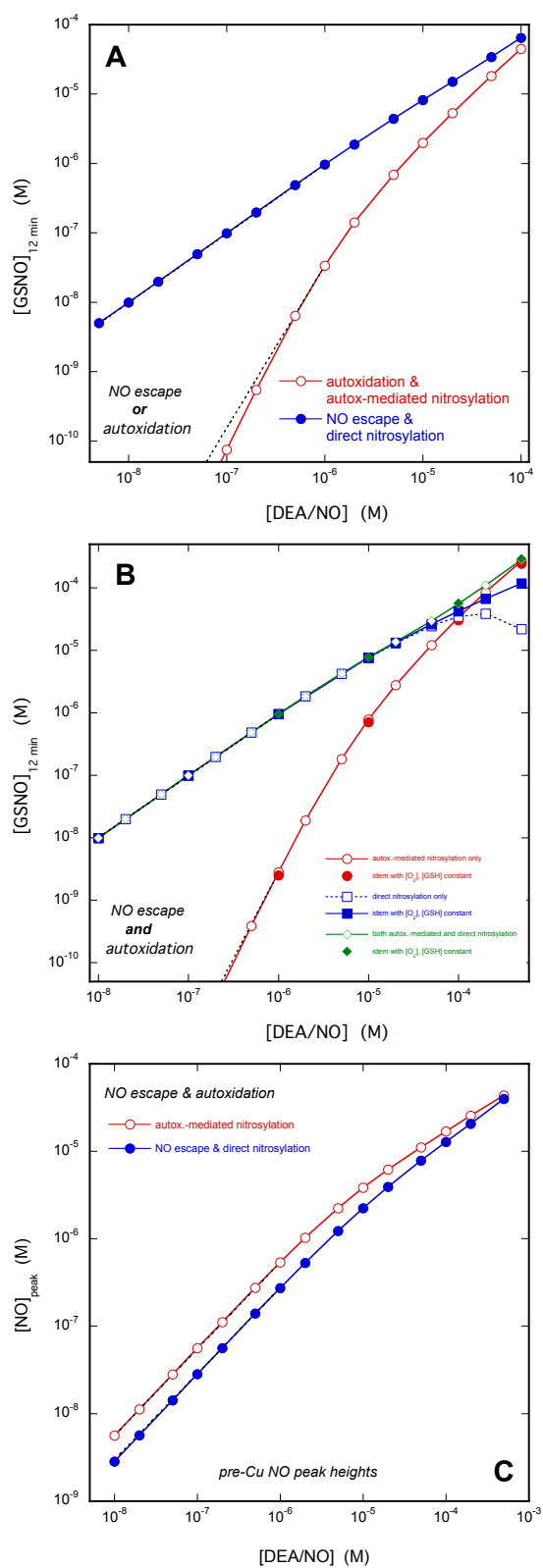
Figure S4. Simulation with Mechanism 2 of the effect of GSH on the concentrations of DEA/NO and its metabolites.
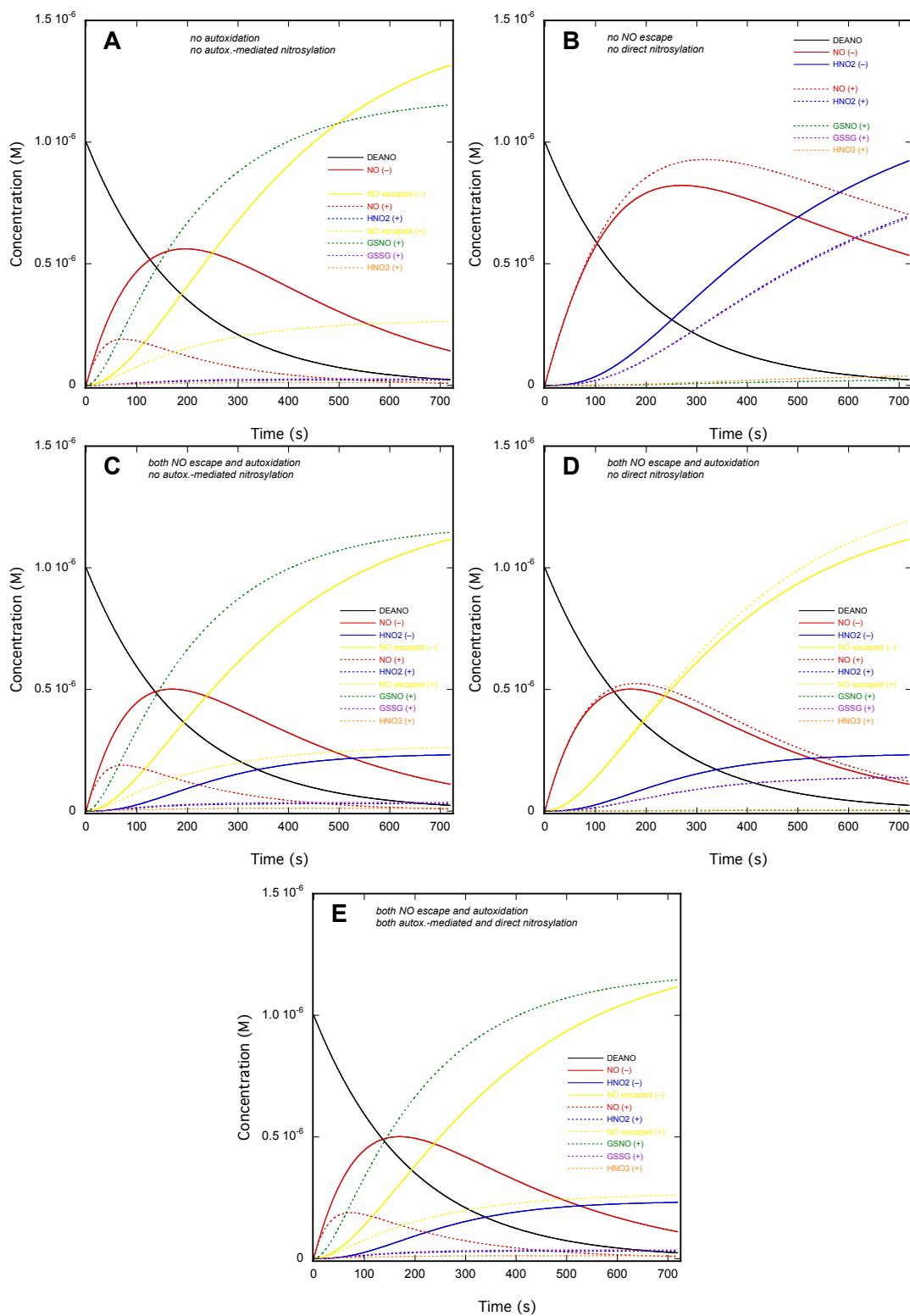
Figure S5. Simulation with Mechanism 2 of the effect of the concentrations of DEA/NO on the height and position of the NO peak.
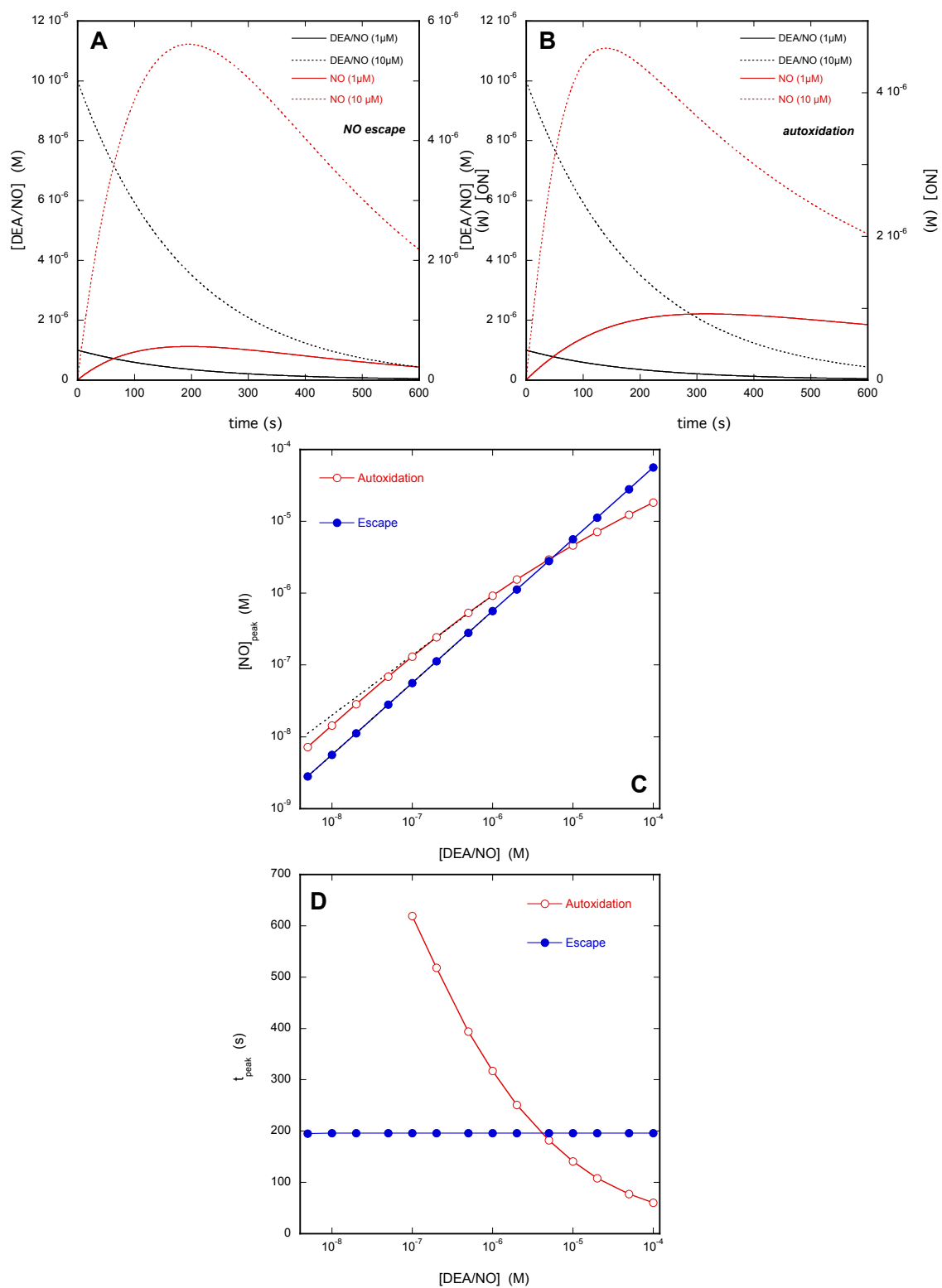
Figure S6. Simulation with Mechanism 2 of the effect of the concentrations of DEA/NO on the GSNO yield after 12 minutes.

Figure S7. Simulation with Mechanism 2 of the effect of omission of SOD on the concentrations of DEA/NO and its metabolites in the presence of GSH.
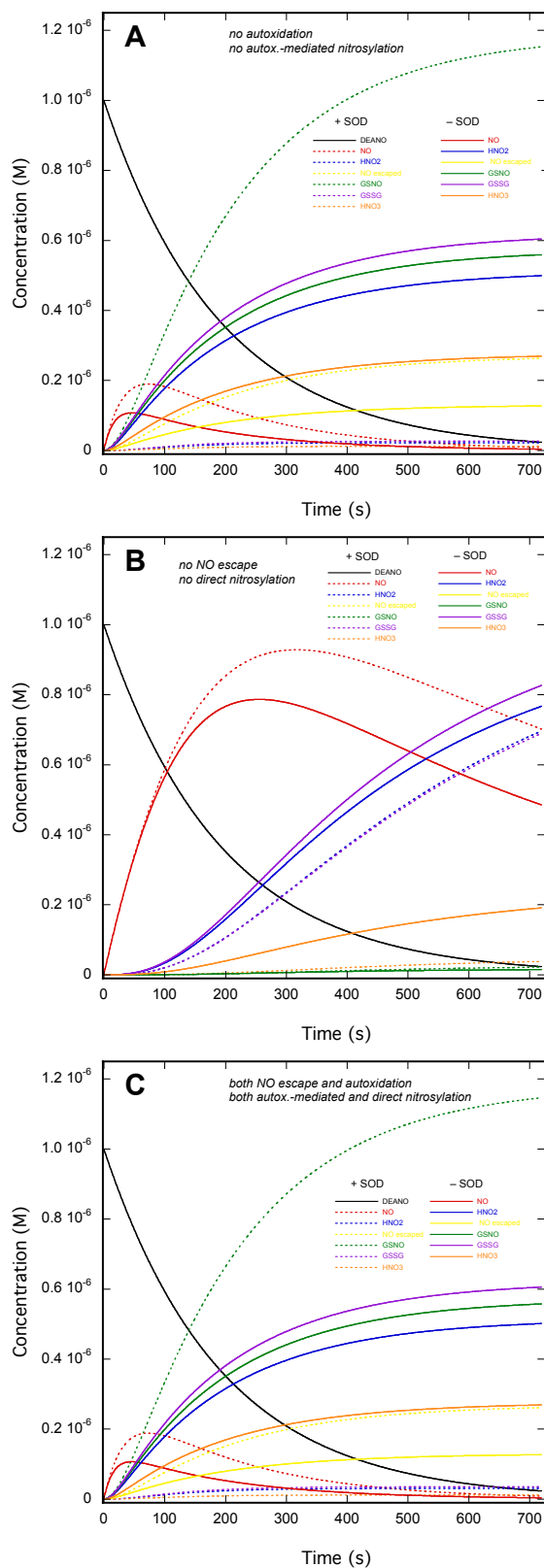
Figure S8. Simulation with Mechanism 2: SOD minimally affects autoxidation-mediated NO peak-heights.
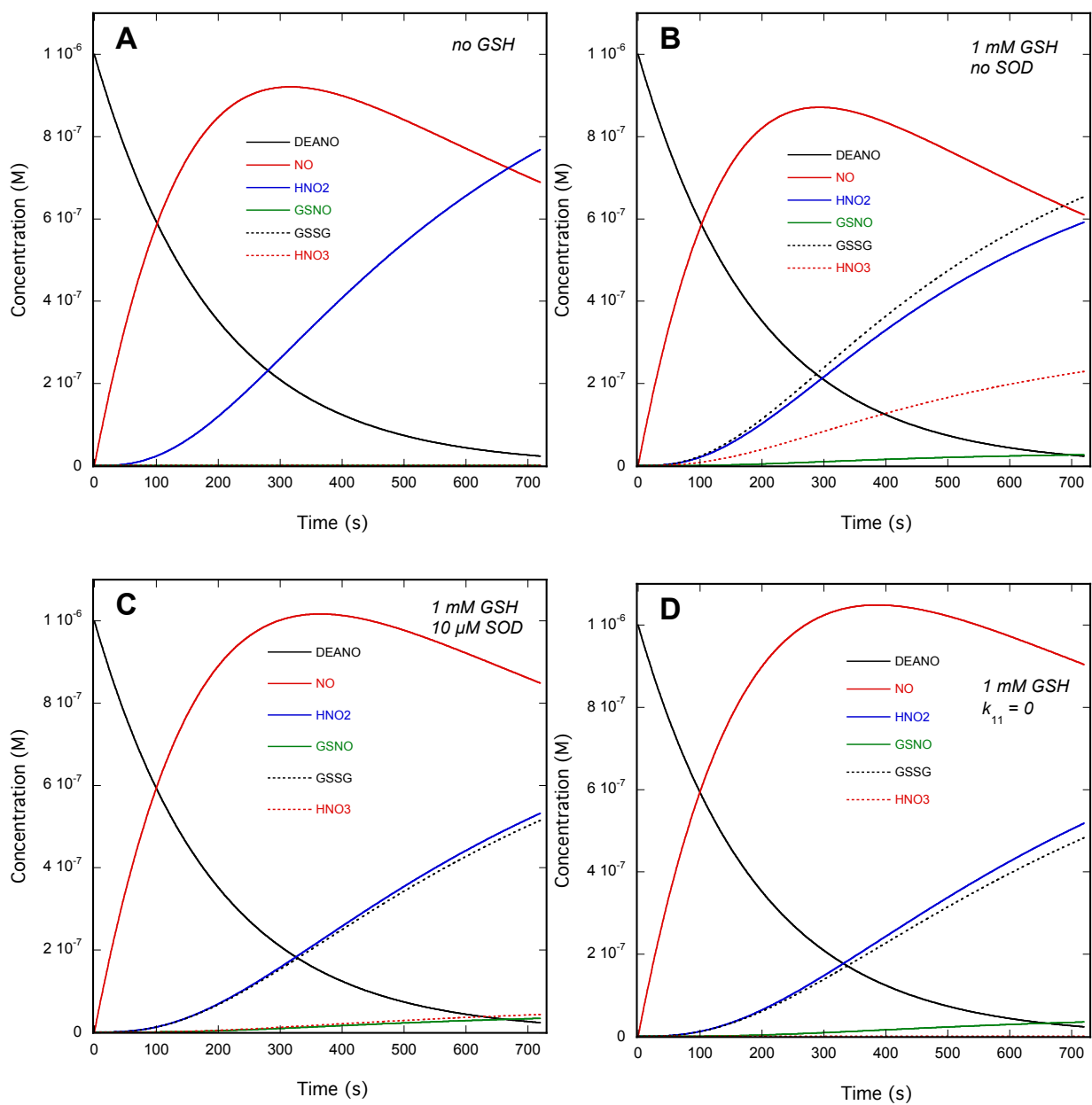
Figure S9. Fits of the observed NO time curves in the absence and presence of GSH.
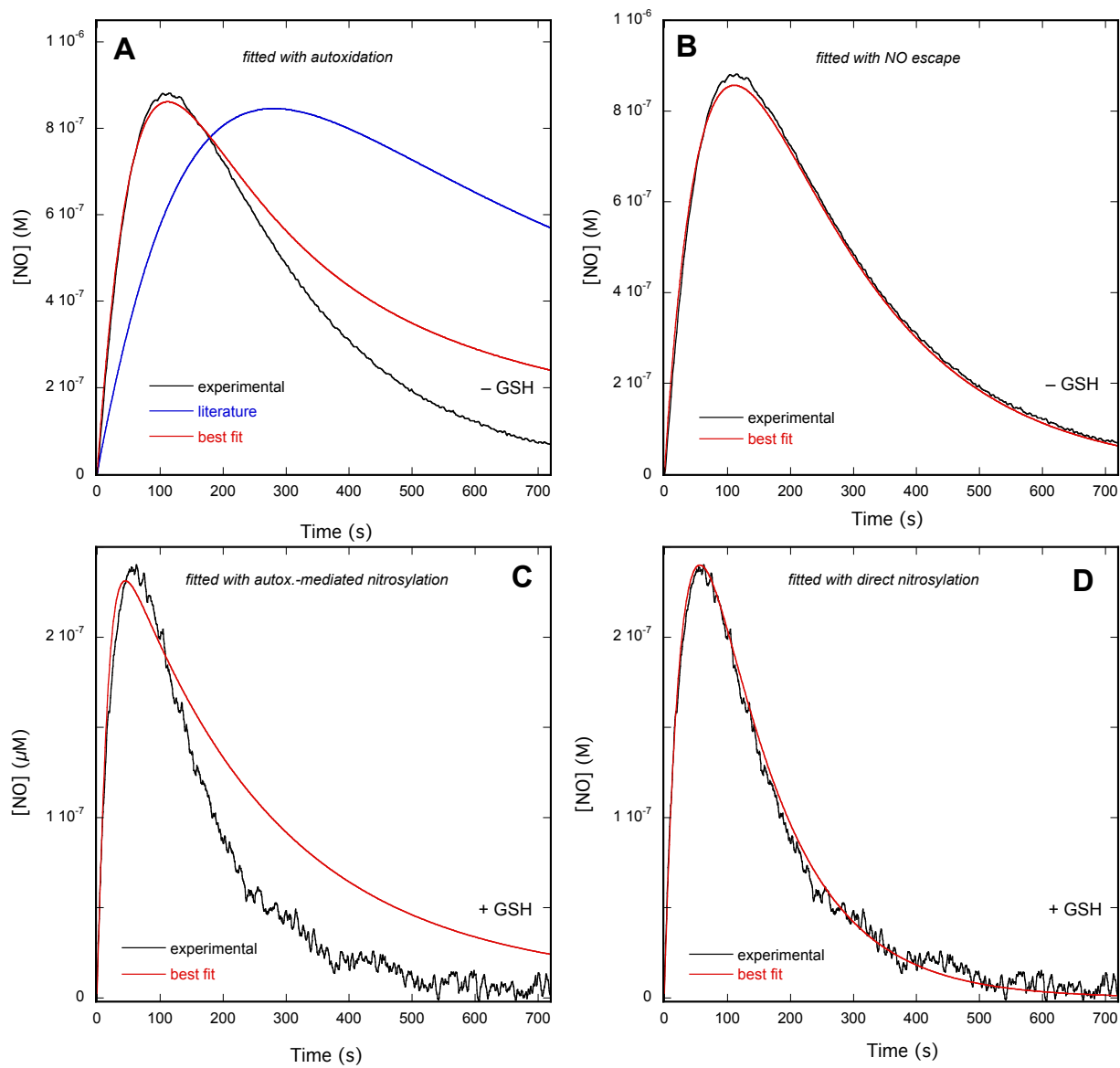
Figure S10. Effect of NAD$^+$ and NADH on pre- and post-Cu^{2+} DEA/NO-derived NO peaks in the absence and presence of GSH.
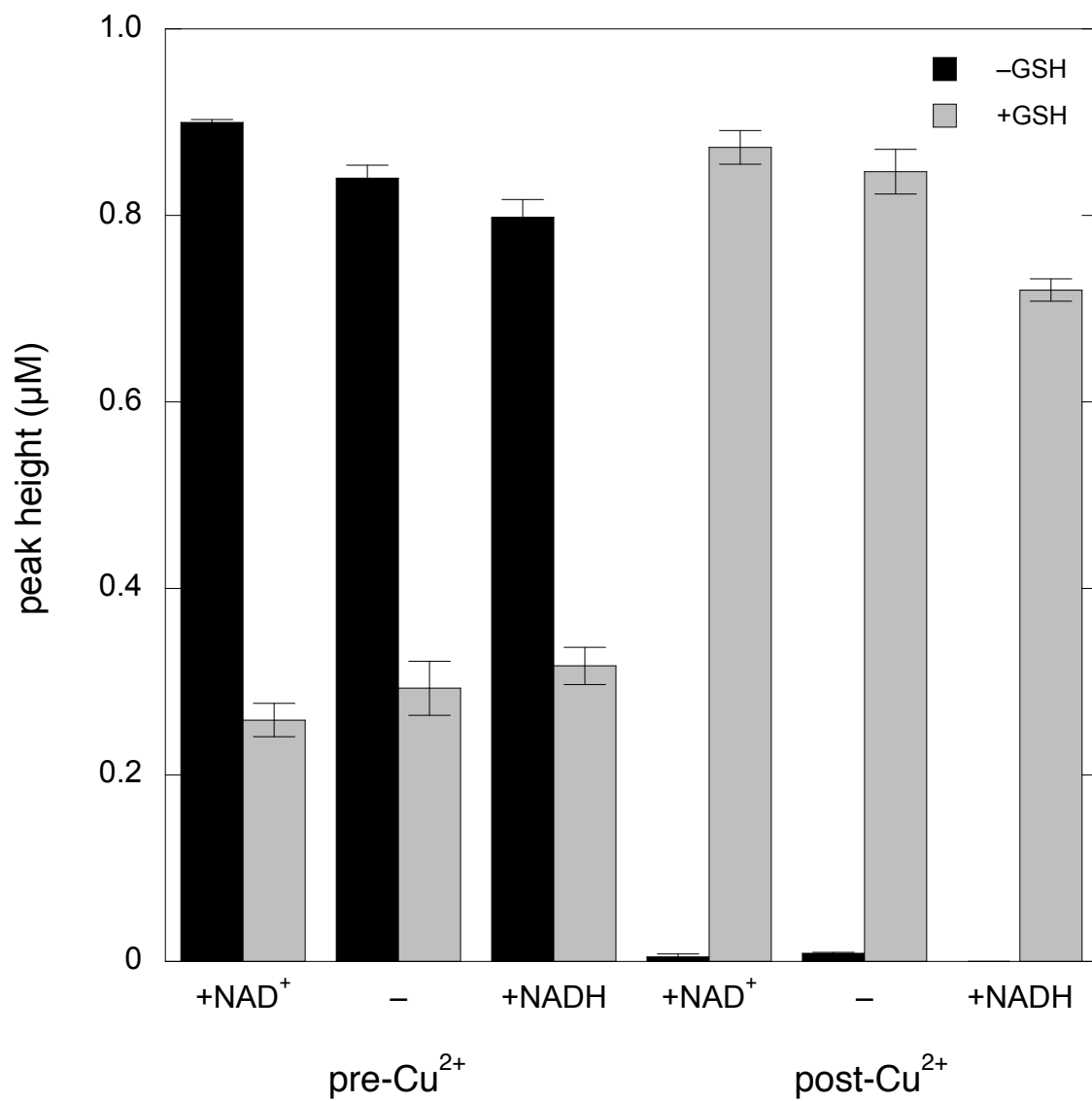
Figure S11A-E. Nitrosation of GSH by glutathione in the presence of NAD$^+$.
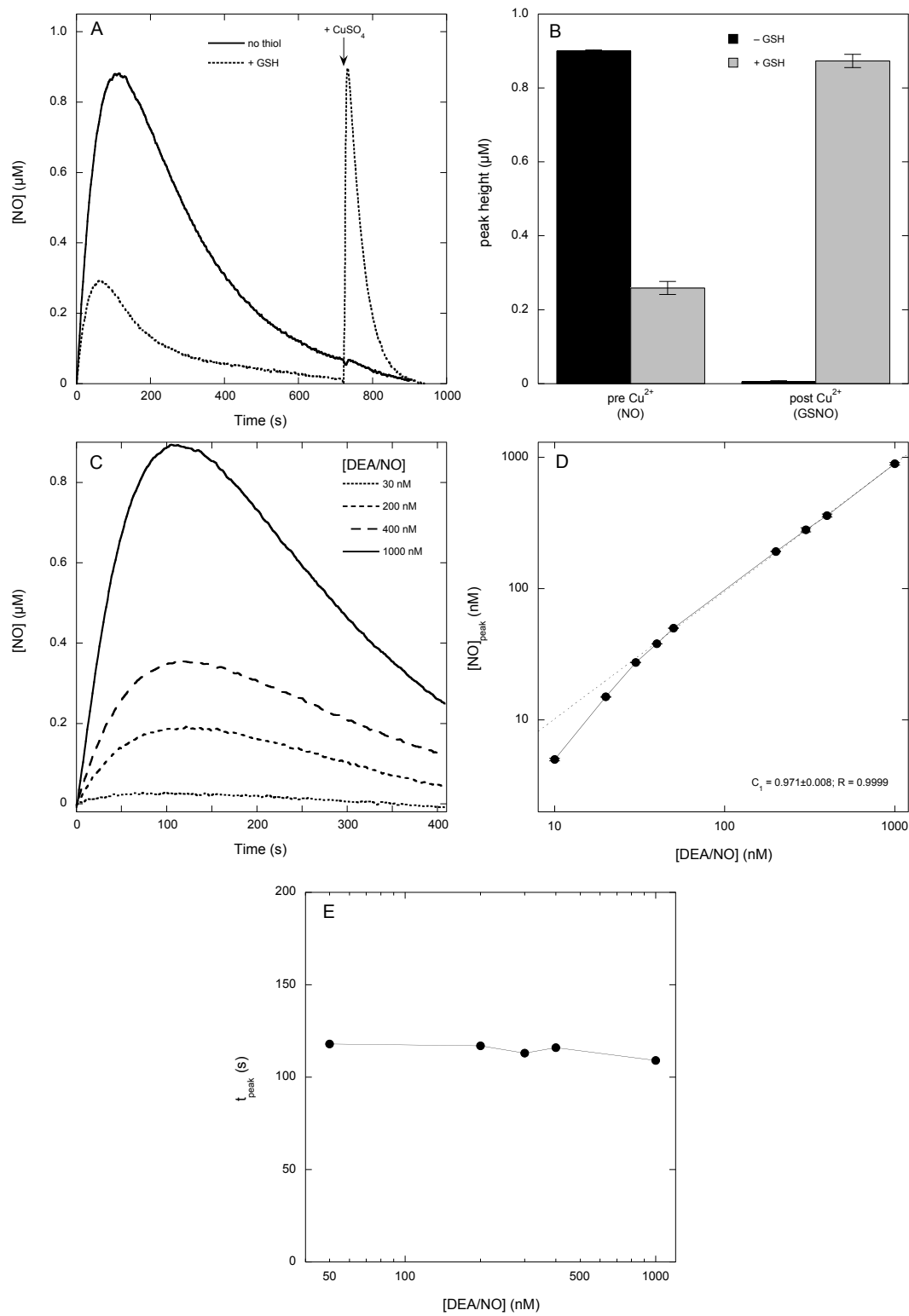
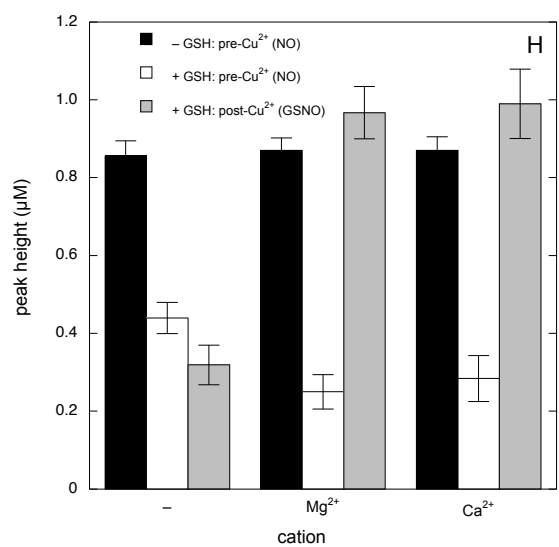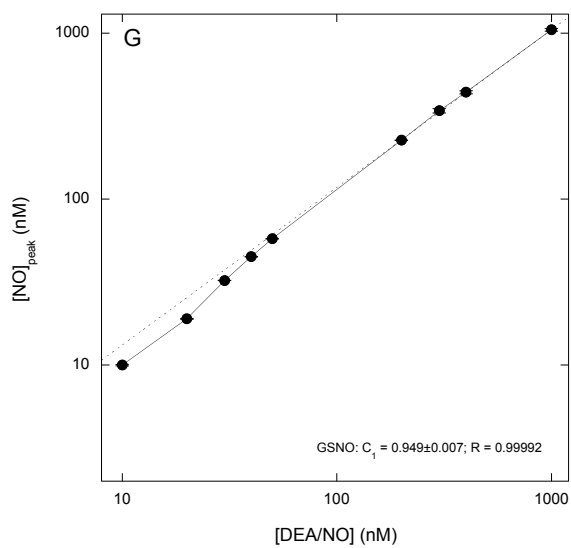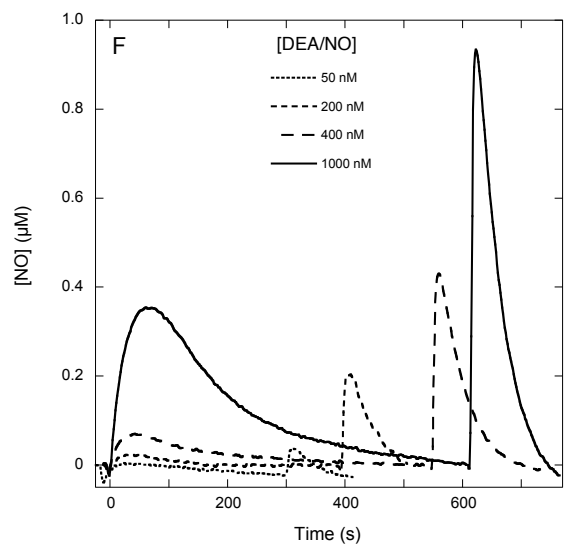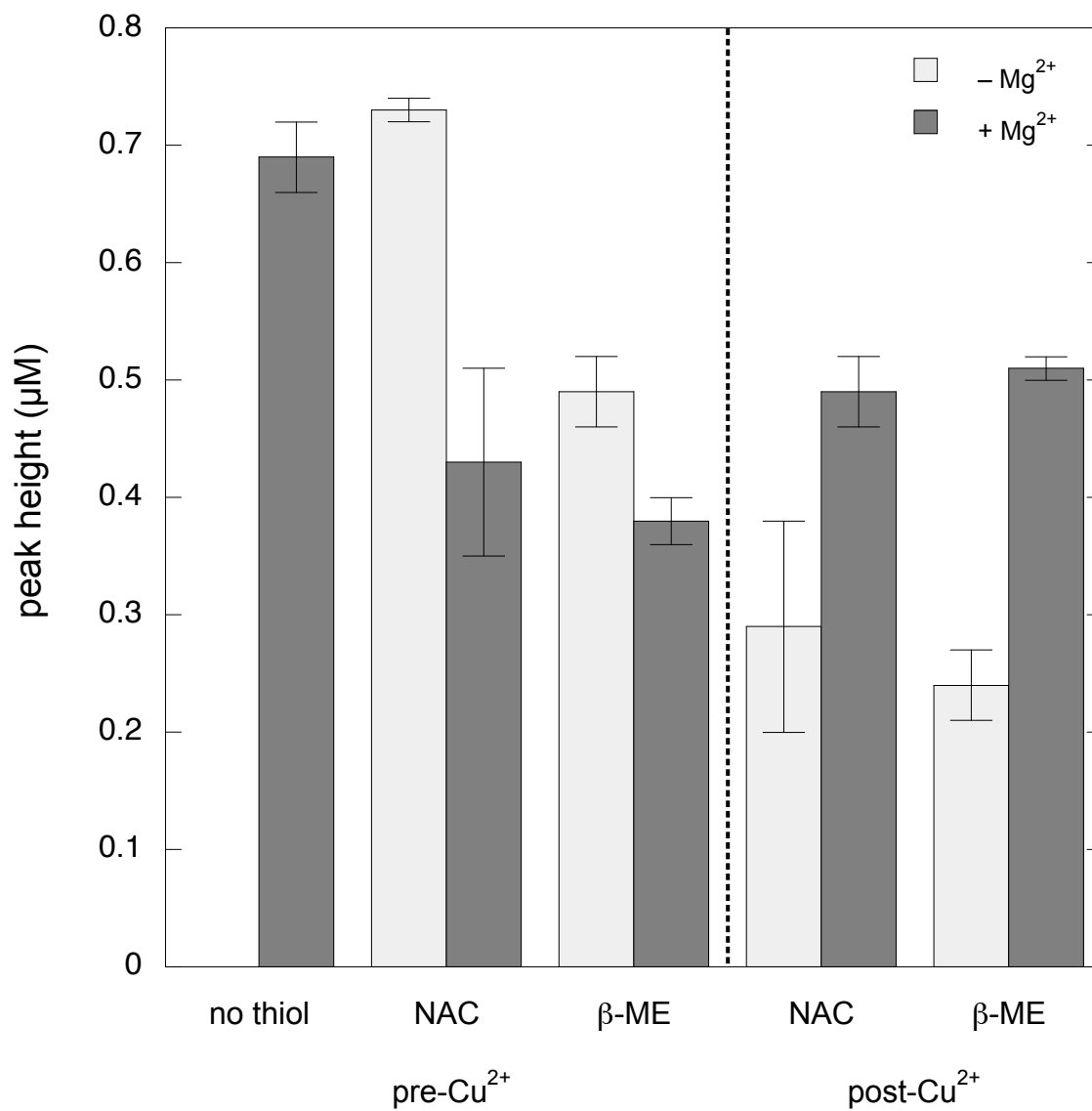**Figure S11F-H. Nitrosation of GSH by glutathione in the presence of NAD$^+$.**

Figure S12. Effect of Mg^{2+} on pre- and post-Cu^{2+} DEA/NO-derived NO peaks in the presence of NAC or β-ME.

Scheme S1. Schematic summary of the reactions considered in the comparison of direct and autoxidation-mediated nitrosation.